Fermilab

FN-333
8000.000

A Search for "Arnol'd Diffusion" in the Beam-Beam Interaction

David Neuffer, Alan Riddiford and Alessandro Ruggiero

April 1981

Abstract

Results and analyses of computer simulations of the beam-beam interaction in the "Tevatron" $\bar{p}p$ collider are presented. Long time simulations of this nonlinear two dimensional (2-D) interaction are undertaken in a search for beam blow-up due to "Arnol'd Diffusion". No large blow-up is seen in simulation of 20 minutes Tevatron time (60 million turns). Limits on the possible magnitudes of emittance increase are presented.

Operated by Universities Research Association Inc. under contract with the Energy Research and Development Administration

Introduction

In the Fermilab "Tevatron I" project, it is planned that bunches of protons and antiprotons will collide in the 1000 GeV superconducting ring, providing high energy particle-antiparticle collisions. When bunches cross each other, single particles are affected by highly non-linear forces generated by the beam bunch moving in the opposite direction.[1]

It has been suggested that such motion could be unstable. The motion of a particle with a periodic, non-linear, two-dimensional (2-D) kick could diverge because of an instability process called "Arnold Diffusion". This phenomenon can occur in the absence of external noise and requires at least two degrees of freedom.[2]

Arnold Diffusion is a slow process, with a rate depending upon the linear beam-beam tune shift $\Delta\nu$, but still possibly serious enough, where it exists, to remove particles from the antiproton ($\bar{p}$) beam in a time period shorter than the required $\bar{p}$ storage time. This effect could endanger the Tevatron I project.

The theory of "Arnold Diffusion" is incomplete. Arnold has demonstrated that a particular nonlinear, 2-D, time dependent dynamical system has an instrinsic instability dependent on the strength of the nonlinearity.[3] The instability causes particle orbits to wander throughout phase space. An hypothesis exists that <u>any</u> 2-D, nonlinear, time dependent, hamiltonian system should exhibit "Arnold Diffusion". This hypothesis has not yet been proven.

The beam-beam interaction is such a system and therefore could exhibit this instability. We have undertaken long-time computer simulations to find evidence for Arnold Diffusion in the beam-beam interaction. We have simulated up to 20 minutes of real Tevatron time (60 million turns) and see no significant evidence of such instability; the motion is stable on that time scale.

The simulations have been performed by use of the Fermilab Cyber computing system with a program originally prepared by Ruggiero[4] and modified by Riddiford. In the following sections we outline the characteristics and the results of these simulations.

Equations of Motion

We consider here only the "weak-strong" case where a test particle in a "weak" beam periodically crosses a "strong" beam. The motion of the particles in the strong beam is not affected by the presence of the weak beam, therefore their charge distribution can be assumed to be constant in time.

The equations of motion of the test particle are

$$\begin{aligned} x'' + K_x(s)\, x &= \frac{-4\pi\Delta\nu_x}{\beta_x^*} F(x,y)\, \delta_p(s)\, x \\ y'' + K_y(s)\, y &= \frac{-4\pi\Delta\nu_y}{\beta_y^*} F(x,y)\, \delta_p(s)\, y \end{aligned} \qquad (1)$$

where x and y are the displacements of the particle motion from a reference orbit (x,y=0), K_x and K_y are the lattice focussing functions and the right hand sides of equations(1) represent the interaction with the strong beam where δ_p is a periodic delta-function of period C.

Equations (1) do indeed describe the motion of a particle in the proton-antiproton colliding beam system at Fermilab, if the following assumptions be taken:

(i). The two unperturbed betatron tune ν_x and ν_y do not depend on the particle momentum. This requires chromaticity cancellation in both planes over a reasonable momentum range.

(ii). The lattice parameters at crossing (α^*, β^*, γ^*) do not depend on the particle momentum over some appreciable range. This might require even higher order corrections than those required to flatten the chromaticity.

(iii). The disperson at the crossing point vanishes over the same momentum range. There is no constraint on the derivative of the dispersion, however.

(iv). Both beams are bunched and the interaction is head-on.

(v). The bunch length in the strong beam is small compared to β^*. In this case it is possible to represent the interaction by a lumped kick; that is, the interaction has infinitesimally small duration which justifies the periodic delta-function at the right hand side of equations(1).

With these assumptions, which approximate physically practical conditions, the interaction between the two beams is independent of the particle momentum and therefore of synchrotron oscillations. In this case one only requires the integration of equations (1) to calculate the motion of a test particle in the "weak" beam.

Our approach is static; that is, we are neglecting all sources of noise which would cause the interaction to fluctuate (gas scattering, intrabeam scattering, power supply noise, quantum fluctuations, etc.).

The proton beam is assumed to have a round, gaussian shape, providing a non-linear force represented by the function

$$F(z) = (1. - DEXP(-z))/z \qquad (2)$$

with

$$z = 75.\ (x^2 + y^2) \qquad (3)$$

where x is the horizontal co-ordinate of an antiproton and y the vertical co-ordinate, with the co-ordinates centered upon the proton beam, and where the units are millimeters.

The root-mean-square size of the proton beam can be found from (3); $75. = 1./(2\sigma^2)$; so that $\sigma = 0.08165$ mm.

It has been proven that if $\alpha_x^* = \alpha_y^*$ and $\nu_x = \nu_y$ and $F(x,y)$ has a symmetry property (see Appendix A), equations (1) can be integrated once, which reduces the number of degrees of freedom from two to one. According to the KAM theorem,[5] if there be only one degree of freedom and the nonlinearity be small enough, the non-linear system cannot be unstable.

The Tevatron I parameters are well described by equations (1) and the above restrictions, except that ν_x need not equal ν_y. (Equations (1) have not been shown to be integrable if $\nu_x \neq \nu_y$.)

Our computer simulations contain two 20 minute real time (60 million turns) Tevatron simulations: one with $\nu_x = \nu_y$ which meets the integrability conditions, the other with $\nu_x \neq \nu_y$.

Computer Simulation Technique

A set of test particles (usually 100) are generated with initial co-ordinates: positions (x,y) and velocities (x',y'), generated randomly following gaussian distributions in each. Those distributions are centered at x=y=x'=y'=0 with dimensions matching the "strong" beam. During generation of initial co-ordinates, co-ordinate sets with a co-ordinate larger than three gaussian standard deviations are rejected and new ones generated.

Since there is a "waist" at the interaction region ($\alpha_x=\alpha_y=0$), the particle "emittances" are

$$\begin{aligned} \varepsilon_x &= \frac{x^2}{\beta_x^*} + \beta_x^* (x')^2 \\ \varepsilon_y &= \frac{y^2}{\beta_y^*} + \beta_y^* (y')^2 \end{aligned} \tag{4}$$

In these simulations we have chosen $\varepsilon_x|_{RMS} = \varepsilon_y|_{RMS}$ and $\beta_x^* = \beta_y^*$, which is equivalent to the condition that both strong and weak beams are "round", as should be true for Tevatron I.

Only one interaction per turn (revolution) is calculated. The simulations have two steps per turn:

1) a linear transformation around the ring;

2) a non-linear kick due to a "beam-beam" interaction.

The linear transformation is modified to include the linear part of the beam-beam interaction. The kicks in the anti-proton velocities are found from:

$$\Delta x' = - \frac{4\pi\Delta\nu}{BTX} \quad F \cdot x$$

$$\Delta y' = - \frac{4\pi\Delta\nu}{BTY} \quad F \cdot y \tag{4A}$$

where $F \to 1$ for small amplitudes x,y and where BTX and BTY are the "before" betas explained below (in the limit $\Delta\nu \to 0$).

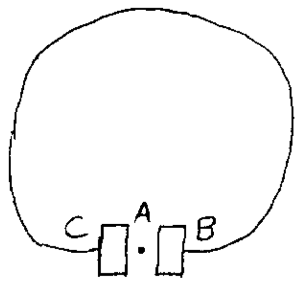

Figure 0. Symmetric Velocity Kicks.

The initial distributions of position and velocity were taken at A. The first velocity kick was one-half the strength given in (4A), and thereafter, when statistics were done on the positions and velocities, one-half of (4A) was subtracted from the velocities, since (4A) takes the antiproton from C to B.

Taking $K = - 4\pi\Delta\nu/\beta$ as the velocity kick for either x or y in (4A), K/2 is applied at the beginning of each turn and K/2 at the end, so (for each plane):

BEFORE

$$\begin{pmatrix} 1 & 0 \\ \frac{K}{2} & 1 \end{pmatrix} \begin{pmatrix} c + \alpha s & \beta s \\ - \gamma s & c - \alpha s \end{pmatrix} \begin{pmatrix} 1 & 0 \\ \frac{K}{2} & 1 \end{pmatrix} =$$

$$= \begin{pmatrix} c + \alpha s + \frac{K}{2}\beta s & \beta s \\ \cdots\cdot & c - \alpha s + \frac{K}{2}\beta s \end{pmatrix} = \begin{pmatrix} c' + \alpha' s' & \beta' s' \\ - \gamma' s' & c' - \alpha' s' \end{pmatrix} \tag{5}$$

AFTER

where the symbols c and s stand for cos $(2\pi\nu)$ and sin $(2\pi\nu)$ and where the unprimed quantities are considered before interaction and the primed quantities after. (We use the linear approximation that $F = 1$.) We desire that the tune of the "after" matrix be matched to the nominal value $\nu_0 = \nu'$ and that β' ("after") be set to the nominal matched value of 2 meters.

The "before" matrix parameters ν, β, α are found by solving the equations

$$\begin{aligned} \alpha = \alpha' &= 0 \\ \cos(2\pi\nu) + \frac{K}{2}\,\beta\sin(2\pi\nu) &= \cos(2\pi\nu_0) \\ \beta\sin(2\pi\nu) &= \beta'\sin(2\pi\nu_0) \end{aligned} \tag{6}$$

with separate equations for x and y, where $\beta'_x = \beta'_y$ is taken but $\nu'_x \neq \nu'_y$ is allowed. With this transformation, the "linear part" of the motion, the motion for small x, is matched to the linear component of the strong beam. With double precision the determinant of the "before" matrix is within 10^{-28} of unity, indicating that the system is conservative for $\lesssim 10^{28}$ turns.

Calculation of the Interaction Form

A. Single precision.

A great deal of computer time can be saved by tabulating interpolation coefficients of the function (2) in one operation at the start of the run. The computer program evaluates F according to

$$F(z) = \begin{cases} g_i(t) & 0 \le z \le 30 \\ 1/z & 30 < z \end{cases} \qquad (7)$$

where $t = z - z_i$, $z_i = (i-1)\Delta z$ defines 12,000 intervals of length $\Delta z = 0.0025$ and where the $1/z$ approximation is adequate to 13 significant digits.

The functions

$$g_i(t) = a_i + b_i t + c_i t^2 + d_i t^3$$

are cubic interpolations whose coefficients a_i, b_i, c_i, d_i for each interval are determined by requiring:

$$\begin{aligned} &1.\quad g_i(0) = F(z_i) \\ &2.\quad g_i(\Delta z) = F(z_i + \Delta z) \\ &3.\quad \frac{d}{dt} g_i(\Delta z/2) = \frac{d}{dz} F(z_i + \Delta z/2) \\ &4.\quad F(z_i + p) - g_i(p) = - F(z_i + \Delta z/2) - g_i(\Delta z/2)) \end{aligned} \qquad (9)$$

where $p = \frac{k}{100} \Delta z$.

All integer values of k from 10 to 40 were tested and k = 35 was chosen which gives the smallest maximum error and with positive and negative errors balanced. The top graph in Figure 1 shows that the approximation is always correct to 12 decimal digits, and to 13 for z greater than about 2.

A computer program evaluating F as in (7) and (8) takes only about 62% of the time that evaluating the function F(z) = (1 -EXP(-Z))/Z takes while giving the same accuracy as the single precision function.

B. Double precision.

For double precision calculations the above interpolation procedure is not adequate. For $z > 0.05$ the function $F(z) = (1 - EXP(-z))/z$ is calculated directly using double precision operations, functions and constants. For $z < 0.05$ a thirteenth order polynominal is used. This obtains F to 28 significant digits.

Repeatability Experiment (Double Precision).

To estimate the accuracy of anti-proton orbits, four particles ($X = Y = \frac{1}{2}\sigma, \sigma, \frac{3}{2}\sigma, 2\sigma$; $X' = Y' = 0$; $\sigma = 0.08165$mm) are simulated on the computer 60 million turns forward and then returned back to their initial starting positions. This requires 9 hours total CPU time. Since anti-protons in the "Doubler" complete 50,000 turns each second, 60 million turns is equivalent to 20 minutes real-ring-time. The computer is less efficient with only four particles, and so the CPU time is 3.2 times the real ring time per particle.

Since $\alpha_x^* = \alpha_y^* = 0$, the reverse run only needs to change the signs of the off diagonal elements (5) and the function F (see (1) and (2)). During the reverse run, positions and velocities are compared with the forward run values. Since $\frac{1}{\beta}X^2 + \beta(X')^2$ is invariant in a linear orbit, the error is estimated by finding the base 10 log of $\sqrt{(\Delta X)^2 + (\beta\Delta X')^2}$ where ΔX and $\Delta X'$ are the differences in X and X' between the forward and backward runs. Since X = Y, only X values are shown in Figure 1A. Orbit positions should be reliable to 14 decimals.

This test guarantees the accuracy of our computer simulation for at least 40 minutes real time in beam-beam, storage ring situations.

Cases Run; Double Precision

Since we want to explore the long-time stability of a storage ring containing both protons and antiprotons, we choose two regions of tune space where there are large resonances which could be expected to enhance instabilities:

$$\text{Case A: } \nu_x = \nu_y = 0.245 \quad , \quad \Delta\nu_x = \Delta\nu_y = 0.01 \quad \text{on-diagonal resonance}$$
$$\text{Case B: } \nu_x = 0.245 \quad \nu_y = 0.12 \; , \; \Delta\nu_x = \Delta\nu_y = 0.01 \quad \text{off-diagonal resonance} \tag{10}$$

Emittance statistic calculations are made after the odd-thousands of turns (1000, 3000, 5000, ...) in groups of 200,000 turns and supergroups of 10 groups. Thirty supergroups were run for a total of 60 million turns or 20 minutes real-ring-time. The 60 million turns required a little under 90 CPU hours. 100 antiproton orbits were calculated, so these runs (2.64 CPU seconds/real-ring- second for each particle) were more efficient than the repeatability runs (3.2 CPU seconds/real ring-second for each particle).

For example, Figure 2 shows emittance statistics for a 64 second simulation on the 1/4 resonance. Each bar summarizes 100 emittance values calculated over 200,000 turns (4 sec.). The top of the bar is the maximum value, the bottom is the minimum value. The line near the center is the best straight line fit to the 100 values. The line across the 16 bars is the best straight line fit for the full 64 sec. run.

Figures 3 and 4 contrast the statistics of rms beam emittances with resonance ($\nu_x = \nu_y = 0.245$) and with a 1/6 resonance ($\nu_x = \nu_y = 0.162$), in 12 second, single precision simulations. XMIT, YMIT (x and y emittances) and

$$\mathrm{RMIT} = \sqrt{\mathrm{XMIT}^2 + \mathrm{YMIT}^2} \qquad (11)$$

are compared.

In Figure 4 we see XMIT and YMIT vary oppositely and their rms sum RMIT remains nearly constant. Figure 3 shows much larger fluctuations, particularly in RMIT. We believe that to be due to the large distortions in particle trajectories due to the 1/4 resonance.

Also, in Figure 2, we notice an immediate increase in emittance from an initial value of 0.0172 mm-mrad to 0.0237 mm-mrad in less than 1000 turns. This "increase" is believed to be caused by a non-linear mismatch. As explained above, ν and β are adjusted to match vanishing-amplitude orbits and initial particles are placed within a gaussian distribution appropriate for a linear force. Large amplitude orbits are unmatched, and this mismatch of resonant orbits generates the initial change in emittance.

Fluctuations in emittance are partially due to statistical fluctuations (only 100 particle orbits) and these statistical fluctuations are enhanced by the large variations in orbits near resonance.

We observe that the calculated emittance presented above,

$$\mathrm{YMIT} = 6 \sqrt{(y - \bar{y})^2 \quad (y' - \bar{y}')^2} \qquad (12)$$

is equivalent to the "95%" emittance of a bigaussian distribution

$$\varepsilon_{95} = 6\,\frac{\sigma^2}{\beta^*} \tag{13}$$

where σ is the rms beam height, and β^* the "beta-function" at the interaction point.

<u>Case A</u>: $\nu_x = \nu_y = 0.245$, $\Delta\nu = 0.010$.

Table I gives the emittance data after every two million turns up to 60 million turns or 20 minutes real-ring-time. After the first row, the values are cumulative, incorporating all the previous data (details are given in Appendix B).

Figure 5 displays the 30 average values for RMIT, each one the average of 1000 emittance values during 2 million turns. The last value for R in Table I is shown on Figure 5 as the horizontal dashed line.

Figure 6 shows the cumulative estimates of the time in days that it would take to change the R emittance by a factor of two. These values are inversely proportional to the cumulative slope estimates of the best straight line fit from t = 0. After the computer run is past 10 minutes real-ring-time (30 million turns) the estimates are all more that 20 days for the RMIT value to decrease to zero.

Figure 7 shows the area of tune of the 1/4 resonance runs. All lines of the form mx + ny = q where m,n,q are integers and where the order ($|m| + |n|$) is less than or equal to 13 which cross the area are shown. Other than the 2nd order line $\nu_y = \nu_x$, there are five 4^{th} order lines, two 6^{th} order lines, six 8^{th} order lines, four 10^{th} order lines and ten 12^{th} order lines.

<u>Case B</u>: $\nu_x = 0.245$, $\nu_y = 0.12$, $\Delta\nu = 0.01$.

Table II gives the emittance data at intervals of two million turns, similar to Table I. The bottom two graphs of Figure 8 display the 30 average values of the x-emittance (XMIT) and y-emittance (YMIT), each one the average of 1000 emittance values during the two million turns. Straight line fits to the data are shown. The top graph of Figure 8 gives the ratio of cumulative slopes of the x-emittance divided by the y-emittance which is equivalent to $\frac{d\varepsilon x}{dt} \Big/ \frac{d\varepsilon y}{dt}$. The appearance of an increase in ε_x matched by a decrease in ε_y suggests some resonance influence which we have not been able to identify precisely.

In Figure 9 the region of tune ($0.245 \lesssim \nu_x < 0.255$, $0.12 \lesssim \nu_y \lesssim 0.13$) for Case B is shown. All resonant lines of order less than 13 are shown. There are single 3^{rd}, 4^{th}, 5^{th} and 6^{th} order resonances, two 7^{th} order resonances, single 8^{th}, 9^{th} and 10^{th} order resonances, three 11^{th} order resonances and three 13^{th} order resonances. Particle orbits with small amplitudes are concentrated near $\nu_x = 0.255$, $\nu_y = 0.13$. Larger amplitude orbits are at lower tune values concentrated near the diagonal $\Delta\nu_x = \Delta\nu_y$.

Figure 10 shows the cumulative estimates of the time in days that it would take to change the x-, y- and R-emittances by a factor of two, found from the inverse of the slopes. After about 12 minutes real-ring-time simulation, the slopes indicate a doubling time of greater than two days. The y-emittance shows a negative "doubling time" indicating a decreasing emittance. This value of doubling time for this case is an order of magnitude smaller than in the previous case of a resonance on the "diagonal" ($\nu_x = \nu_y$). This suggests that Case A is more stable than Case B.

Single Precision Runs

The same cases (A and B) were also run in single precision simulations, where ten supergroups are needed to complete the 60 million turns or 20 minutes real-ring-time. Each supergroup is 6 million turns or 30 groups of 200,000 turns. Each supergroup ran a little over two CPU hours, so that the complete run required almost 22 hours.

The matrix calculations take about 1/3 of the CPU time, the other 2/3 being required by the cubic interpolation of the interaction function F. Quadratic or even linear approximations can be used and will speed up the runs, but accuracy will suffer and the number of intervals required will increase.

Figure 11 explains why we went to double precision. The repeatability experiment (similar to Figure 1 for double precision) showed errors in the orbit positions comparable with the positions themselves after 20 million turns.

Table III compares the single precision results with the double precision results. The Case B run was stopped at 30 million turns (10 minutes real-ring-time).

The statistics used for single precision runs were different from that explained above for the double precision runs, so the doubling times do not use the same data, and so should not be precisely the same. In single precision runs emittance values were taken at the even thousands (0, 2000, 4000, ...) which meant counting the emittance at the end of each group twice.

After each of the 30 double precision supergroups, a comparison was made of ten x-values and ten y-values with the single precision values. On the average the case A run differed by more than 1 in the 5^{th} decimal at two million turns and in the 3^{rd} decimal at 60 million turns. The Case B run was only slightly worse.

Both single and double precision cases yield the same rate of change for Case A and the same magnitude of change for Case B.

Conclusion

We have made two long-run simulations of the beam-beam interaction for a geometry which we believe to be a good approximation of Tevatron $\bar{p}p$ colliding beams.

In Case A ($\nu_x = \nu_y = 0.245$) we find stability. Our result is that it requires ~20 days for the beam emittance to double and this result is consistent with the theorem on integrability of this system (Appendix A).

In Case B ($\nu_x \neq \nu_y$) we find that the weak emittance can change by a factor of two in two days and this result is statistically significant (Appendix C). This may be "Arnold Diffusion", but it is a small effect for $\bar{p}p$ parameters.

We plan to extend these runs to 120 to 200 million turns (40 to 60 minutes real-ring-time) to set further limits on "Arnold Diffusion". We also hope to explore other beam-beam geometries, such as collisions of elliptical rather than circular beams, and also the effects of "tune modulation".

References

1. J.C. Herrera, "Electromagnetic Interaction of Colliding Beams in Storage Rings", AIP Conf. Proceedings on Non-Linear Dynamics and the Beam-Beam Interaction, edited by M. Month and J.C. Herrera - BNL, 1979, pages 29-41.

2. B.V. Chirikov, Physics Report Vo. 52, No. 5, 1979, pages 263-379.

3. V.I. Arnold, Dokl. Akad. Nauk SSSR 156 (1964) 9.

4. A.G. Ruggiero, IEEE Trans. on Nucl. Science, Vol. NS-24, No. 3, June 1977.

5. J. Moser, "Stable and Random Motions in Dynamical Systems", Annals of Mathematics Studies, No. 77, Princeton University Press, New Jersey, 1973.

6. P.R. Bevington, Data Reduction and Error Analysis for the Physical Sciences, McGraw-Hill, New York, 1969, p. 114.

Appendix A. Integrability Theorem

Let us write the equations of motion (1) in the form:

$$x'' + k_x(s)\ x = \xi_x F_x(x,y)\,\delta_p(s) \tag{1A}$$
$$y'' + k_y(s)\ y = \xi_y F_y(x,y)\,\delta_p(s)$$

Theorem: If the following conditions be satisfied:

$$\nu_x = \nu_y \qquad \text{and} \qquad \alpha^*_x = \alpha^*_y \tag{2A}$$

then there exists an infinite variety of strong beam charge distributions for which the original equations of motion (1A) admit at least one integral of motion.

Proof: The interaction force can be derived from a potential function:

$$\xi_x F_x(x,y) = -\frac{\partial U}{\partial x} \qquad \text{and} \qquad \xi_y F_y(x,y) = -\frac{\partial U}{\partial y} \tag{3A}$$

The pair of equations (1A) can then be obtained from the following hamiltonian:

$$H = \frac{p_x^2 + p_y^2}{2} + \frac{k_x x^2 + k_y y^2}{2} + U(x,y)\,\delta_p(s) \tag{4A}$$

This is a non-autonomous system with two degrees of freedom. The independent variable is s; the canonically conjugate variables are:

$$x,\ p_x = x' \qquad \text{and} \qquad y,\ p_y = y' \tag{5A}$$

According to Maxwell's equations, the potential U is related to the charge distribution $\rho(x,y)$ in the strong beam by the Poisson's equation:

$$\nabla^2 U(x,y) = \rho(x,y) \tag{6A}$$

Let $\mu_x = 2\pi\nu_x$ and $\mu_y = 2\pi\nu_y$ be the betatron phase advances in the two planes between two consecutive crossings. Whether there be only one or more than one interaction per revolution is immaterial here, provided that the lattice repeats identically between crossings.

It is well known that in the limit $\xi_x = \xi_y = 0$ the position and angle of the test particle after the n-th crossings are given by:

$$x_n = \sqrt{\varepsilon_x \beta_x^*} \cos(n\mu_x + \delta_x)$$
$$x'_n = -\sqrt{\frac{\varepsilon_x}{\beta_x^*}} \left\{ \alpha_x^* \cos(n\mu_x + \delta_x) + \sin(n\mu_x + \delta_x) \right\} \qquad (7A)$$

and similarly for y_n and y'_n. In equations (7A) ε_x and δ_x are two constants of motion. The first one measures the amplitude of the motion.

Let us make the following change of variables:

$$\underset{\text{old}}{(x,x';y,y')} \qquad \underset{\text{new}}{(r,p_r;\theta,p_\theta)} \qquad (8A)$$

with

$$x = \sqrt{r\beta_x^*} \cos\theta \qquad \text{and} \qquad y = \sqrt{r\beta_y^*} \sin\theta \qquad (9A)$$

The generating function for this transformation is:

$$S(\theta,r;p_x,p_y) = \left\{ xp_x + yp_y \right\}$$
$$= x'\sqrt{r\beta_x^*} \cos\theta + y'\sqrt{r\beta_y^*} \sin\theta \qquad (10A)$$

from which we derive the new momenta:

$$p_\theta = -\frac{\partial S}{\partial \theta} \qquad \text{and} \qquad p_r = \frac{\partial S}{\partial r} \qquad (11A)$$

p_θ is similar to angular momentum:

$$p_\theta = x'\sqrt{r\beta_x^*}\ \sin\theta - y'\sqrt{r\beta_y^*}\ \cos\theta$$

$$= \sqrt{\frac{\beta_x^*}{\beta_y^*}}\ x'y - \sqrt{\frac{\beta_y^*}{\beta_x^*}}\ y'x \tag{12A}$$

We calculate p_θ at the interaction point after n crossings in the limit $\xi_x = \xi_y = 0$. Inserting (7A) and similar equations for y,y' into (12A) we obtain

$$p_{\theta n} = \sqrt{\varepsilon_x\varepsilon_y}\ \sin\ (\delta_y - \delta_x) \tag{13A}$$

which is a constant, an invariant of motion.

Let us see now the effect of the kick with ξ_x and $\xi_y \neq 0$:

$$\Delta x_n = 0 \qquad\qquad \Delta y_n = 0$$

$$\Delta x'_n = \xi_x F_x(x_n, y_n) \qquad \Delta y'_n = \xi_y F_y(x_n, y_n)$$

We have:

$$\Delta p_{\theta n} = \sqrt{\frac{\beta_x^*}{\beta_y^*}}\ y_n \Delta x'_n - \sqrt{\frac{\beta_y^*}{\beta_x^*}}\ x_n \Delta y'_n$$

$$= \sqrt{\frac{\beta_x^*}{\beta_y^*}}\ y_n \xi_x F_x(x_n, y_n) - \sqrt{\frac{\beta_y^*}{\beta_x^*}}\ x_n\ {}_y F_y(x_n, y_n)$$

$$= -\sqrt{\frac{\beta_x^*}{\beta_y^*}}\ y_n \left(\frac{\partial U}{\partial x}\right)_n + \sqrt{\frac{\beta_y^*}{\beta_x^*}}\ x_n \left(\frac{\partial U}{\partial x}\right)_n$$

After the transformation (9A) is applied:

$$U = U(x,y) \rightarrow U(r,\theta)$$

It is obvious that if $\partial U/\partial\theta = 0$, i.e. the potential depends only on the "radial" coordinate r,

$$\frac{\partial U}{\partial x} = \frac{dU}{dr}\frac{\partial r}{\partial x} = 2\,\frac{x}{\beta^*_x}\,\frac{dU}{dr}$$

$$\frac{\partial U}{\partial y} = \frac{dU}{dr}\frac{\partial r}{\partial y} = 2\,\frac{y}{\beta^*_y}\,\frac{dU}{dr}$$

then $\Delta p_{\theta_n} = 0$, that is p_θ remains a constant of motion with the beam-beam interaction.

From (9A) we obtain:

$$r = \frac{x^2}{\beta^*_x} + \frac{y^2}{\beta^*_y}$$

If U be a function of only this variable, then we have from (6A) that all charge distributions satisfying the equation

$$\rho(x,y) = 4\left(\frac{x^2}{\beta^{*2}_x} + \frac{y^2}{\beta^{*2}_y}\right)\frac{d^2U}{dr^2} + 2\left(\frac{1}{\beta^*_x} + \frac{1}{\beta^*_y}\right)\frac{dU}{dr} \qquad (14A)$$

with any arbitrary U=U(r), satisfy also the requirements of the theorem.

In particular if $\beta^*_x = \beta^*_y$ and the strong beam is "round", as is approximately true for the $p\bar{p}$-project at Fermilab, then a gaussian charge distribution in the strong beam is consistent with the assumptions and the theorem.

Discussion

As we have already mentioned, equations (1A) represent a system with two non-autonomous degrees of freedom. This has been conjectured to be a sufficient and necessary condition for the system to be affected by Arnold diffusion: an instability caused by the intersection (not over-lapping) of the non-linear resonances in the four-dimensional phase space.

Bet we have just proven with the previous theorem that if the conditions (2A) and (14A) are satisfied, the system can admit one integral of motion, p_θ given by equation (12A). Therefore equations (1A) can be integrated at least once. One can eliminate θ as a variable, and the motion of the test particle can be reduced to one degree of freedom. In this case the KAM theorem[5] insures that for small values of the perturbation (ξ_x and ξ_y) the motion is bounded by stable trajectories.

In this case (p_θ=constant), the resonances in the four dimensional phase space never intersect with each other. The question remains whether this is generally true or requires conditions (2A) and (14A). If this be true, then the beam-beam interaction cannot exhibit Arnold diffusion.

Appendix B. Best Straight Line Fit of Emittance Values

In this section we describe our method of calculating the slope from our sets of emittance values.

As shown in the "BAR" part of Figure 12, 100 emittance values are taken at the odd thousands of turns (100, 300, ..., 199,000). The SLOPE is found from

$$\text{SLOPE} = \frac{\Sigma xy - (\Sigma x)(\Sigma y)}{\Sigma x^2 - (\Sigma x)^2} \tag{1B}$$

Scaling each bar to $0 \leq x \leq 1$, SL, defined in Figure 12, was found from:

$$100{,}000 \text{ SLOPE} = SL/2 = DY \tag{2B}$$

To find the best straight line fit to the ten (N=10) "BARS" making up a "GROUP" (see Figure 12)

$$\begin{aligned} x &= \bar{x}_i - \tfrac{1}{2} + \frac{j - 0.5}{100} \qquad j=1,2,\ldots,100 \\ y &= \bar{y}_i + SL_i \left(-\tfrac{1}{2} + \frac{j - 0.5}{100}\right) \end{aligned} \tag{3B}$$

and the overall ΔY, always using a zero x-average was found from

$$\Delta Y = \frac{N}{2} \frac{\frac{1}{100} \Sigma xy}{\frac{1}{100} \Sigma x^2} \tag{4B}$$

where the numerator is made up of N sums like:

$$\frac{1}{100} \sum_{j=1}^{100} \left(\bar{x}_i - \tfrac{1}{2} + \frac{j-0.5}{100}\right) \left[\bar{y}_i + SL_i \left(-\tfrac{1}{2} + \frac{j-0.5}{100}\right)\right] \tag{5B}$$

and the denominator sums all the points:

$$\frac{1}{100} \Sigma\, x^2 = \frac{1}{100} \sum_{j=1}^{100N} \left(-\frac{N}{2} + \frac{j - 0.5}{100}\right)^2 \tag{6B}$$

Since:

$$\sum_1^k i = \tfrac{1}{2}k\,(k + i) \tag{7B}$$

$$\sum_1^k i^2 = \frac{k}{6}\,[1 + k\,(3 + 2k)] \tag{8B}$$

(5B) becomes:

$$(\bar{x}_i - \tfrac{1}{2} - \tfrac{1}{200})(\bar{y}_i + SL_i\ [-\tfrac{1}{2} - \tfrac{1}{200}])$$

$$+ \left[\bar{x}_i - \tfrac{1}{2} - \tfrac{1}{200} + \bar{y}_i + SL_i\ (-\tfrac{1}{2} - \tfrac{1}{200})\right. \quad \frac{101}{200}$$

$$+ SL_i \frac{(1 + 100 \cdot 203)}{100 \cdot 100 \cdot 6}$$

$$= \bar{y}_i \cdot \bar{x}_i + \frac{1 - 0.0001}{12} SL_i \tag{9B}$$

The sum (6B) becomes:

$$\frac{1}{100} \sum_{j=1}^{100N} \left(\frac{N^2}{4} - N \left\{\frac{j - 0.5}{100}\right\} + \frac{j^2 - j + 0.25}{10^4}\right)$$

$$= \frac{N^3}{4} + \frac{N^2}{200} + \frac{N}{4 \cdot 10^4} - \left(\frac{N}{100} + \frac{1}{10^4}\right) \frac{N}{2} (100N + 1)$$

$$+ \frac{N(1 + 100N\ (3 + 200N))}{6 \cdot 10^4} = (N^3 - N \cdot 10^{-4})/12 \tag{10B}$$

The quantity ΔY in (4B) becomes:

$$\Delta Y = \frac{\sum_{i=1}^{N} (\bar{y}_i \cdot \bar{x}_i + 0.16665 \cdot 10^5 \cdot SLOPE_i)}{(N^2 - 10^{-4})/6} \tag{11B}$$

The supergroup calculations are very similar, except the sums are over 1000 values instead of 100. The slope SL_i in (3B) is replaced by $\Delta Y/(1/2)=2\Delta Y$ so that:

$$x = xB_i - \frac{1}{2} + \frac{j - 0.5}{1000} \qquad j = 1,2,\ldots,1000$$

$$y = yB_i + 2\Delta Y_i \left(-\frac{1}{2} + \frac{j - 0.5}{1000}\right) \tag{12B}$$

The supergroup slope can be found from:

$$\delta Y = \frac{\sum_{i=1}^{L} (\bar{y}_i \cdot \bar{x}_i + 0.1666665 \cdot \Delta Y_i)}{Y_i \ (L^2 - 10^{-6})/6} \qquad (13B)$$

To find the doubling time YMIN, the supergroup slope is found by dividing δY by the number of minutes in L/2 groups. Since each group is 2/3 minutes, the doubling time is found from:

$$Y_{AV} = \frac{\delta Y}{\frac{L}{2} \cdot \frac{2}{3}} \cdot Y_{MIN} \qquad (14B)$$

or

$$Y_{MIN} = \frac{Y_{AV} \cdot L}{3 \cdot \delta Y} \qquad (15B)$$

Appendix C. The Statistical Significance of the Calculated Slopes

P.R. Bevington[6] gives an estimate for the error in the slope (2B) to be:

$$\sigma_b^2 = \frac{N\ s^2}{N\Sigma x_i^2 - (\Sigma x_i)^2} \tag{1C}$$

where:

$$s^2 = \frac{1}{N - 2}\ \Sigma\ (y_i - a - bx_i)^2 \tag{2C}$$

Emittance values were printed, and to do the sum in (2C) including all 30,000 emittance values would require days of keypunching. The above expression for σ_b can be shown to scale as

$$\sigma_b \propto 1/\sqrt{N} \tag{3C}$$

as the number of points (x_i, y_i) is increased, if the y_i follow a normal distribution about the linear fit. We can find the error for a subset of the 30,000 values and scale to find the error for the full set. In order to check this scaling, 3000 values of RMIT (Case A) were keypunched (at turns 9000; 29,000; 49,000;...59,969,000; 59,989,000) and σ_b was found to be:

$$\sigma_b = 4.49 \times 10^{-6}\ \frac{\text{mm-mrad}}{\text{mm}} \quad \text{(3000 data points, RMIT, Case A)} \tag{4C}$$

Then every tenth value was used for a series of ten sums (1C) and (2C) using only 300 values, starting with the 1st value, then for the next set starting with the 2nd value, then 3rd,...10th value. The average of the ten estimates of DS using only 300 points was:

$$\sigma_b = 1.42 \times 10^{-5}\ \text{min}^{-1} \quad \text{(average of 10 sets of 300 data points, RMIT, Case A)} \tag{5C}$$

To check the scaling (3C), multiply (4C) by $\sqrt{10}$:

$$\sqrt{10} \times 4.49 \times 10^{-6} = 1.42 \times 10^{-5}\ \frac{\text{mm-mrad}}{\text{min}} \tag{6C}$$

The estimate for the slope error σ_b using all 30,000 emittance values is therefore

$$4.49 \times 10^{-6}/\sqrt{10} = 1.42 \times 10^{-6}\ \frac{\text{mm-mrad}}{\text{min}} \quad \text{(30,000 data points, RMIT, Case A)} \tag{7C}$$

Any slope within the band $\pm$(7C) is expected to be statistically indistinguishable from a zero shape.

In order to compare (7C) with the doubling time of -54 days on Table I after 60 million turns:

$$R_{av} = 1.42 \times 10^{-6}\ \Delta t \tag{8C}$$

$$\Delta t = 0.0336/1.42 \times 10^{-6} = 23662 \text{ min or } 16.4 \text{ days} \tag{9C}$$

Any doubling time longer than 16.4 days is expected to be statistically indistinguishable from an infinite doubling time (or a zero slope).

Since 54 days is almost four times longer than 16.4 days, our data for R-emittance (Case A) is statistically indistinguishable from a zero slope.

For Case B the numbers were:

	σ_b (300 values) mm-mrad/min	σ_b (30000 values) mm-mrad/min	Δt	Table II Doubling Time	
x	1.319×10^{-5}	1.319×10^{-6}	12 days	1.3 days	
y	4.605×10^{-6}	4.605×10^{-7}	29 days	-5.4 days	(10C)
R	1.049×10^{-5}	1.049×10^{-6}	20 days	2.7 days	

The doubling times on Table II after 60 million turns are all from 5 to 9 times shorter than the $\pm\Delta t$ band.

So our data on Table II show (statistically) significantly non-zero slopes.

As further runs are made, all emittance values will be made available for a more accurate estimate of σ_b in (1C) and (2C).

TABLE I. Emittance data for Case A; $\nu_x = \nu_y = 0.245$; $\Delta\nu = 0.010$
Cumulative values.

Real Ring Time (min)	Million turns	X_{av}	Doubling Time (days)	Y_{av}	Doubling Time (days)	R_{av}	Doubling Time (days)
$\frac{2}{3}$	2	0.0237166	0.3	0.0236805	-0.3	0.0336119	-1.5
$1\frac{1}{3}$	4	0.0237070	1.6	0.0236929	-2.5	0.0336144	1.9
2	6	0.0236984	-0.8	0.0236972	1.3	0.0336123	-6.7
$2\frac{2}{3}$	8	0.0237149	0.8	0.0236935	-3.1	0.0336211	2.0
$3\frac{1}{3}$	10	0.0237005	-2.0	0.0237146	.6	0.0336278	1.3
4	12	0.0237104	2.2	0.0237039	3.5	0.0336288	1.8
$4\frac{2}{3}$	14	0.0237044	-12.	0.0237051	3.9	0.0336267	4.1
$5\frac{1}{3}$	16	0.0237062	28.	0.0237028	41.	0.0336267	6.7
6	18	0.0237050	-21.	0.0237059	5.4	0.0336277	7.1
$6\frac{2}{3}$	20	0.0237085	6.3	0.0237017	-13.	0.0336277	9.2
$7\frac{1}{3}$	22	0.0236997	-3.5	0.0237084	4.1	0.0336267	22.
8	24	0.0237051	-170.	0.0237027	-23.	0.0336262	50.
$8\frac{2}{3}$	26	0.0237059	30.	0.0237036	-220.	0.0336272	25.
$9\frac{1}{3}$	28	0.0237055	92.	0.0237060	11.	0.0336286	14.
10	30	0.0237051	-330.	0.0237034	-83.	0.0336263	190.
$10\frac{2}{3}$	32	0.0237058	42.	0.0237015	-13.	0.0336256	-92.
$11\frac{1}{3}$	34	0.0237026	-13.	0.0237045	41.	0.0336256	-96.
12	36	0.0237030	-18.	0.0237047	36.	0.0336253	-67.
$12\frac{2}{3}$	38	0.0237054	58.	0.0237013	-15.	0.0336249	-50.
$13\frac{1}{3}$	40	0.0237024	-16.	0.0237028	-50.	0.0336243	-33.
14	42	0.0237038	-50.	0.0237011	-17.	0.0336241	-35.
$14\frac{2}{3}$	44	0.0237033	-36.	0.0237020	-30.	0.0336246	-58.
$15\frac{1}{3}$	46	0.0237033	-42.	0.0237019	-34.	0.0336244	-58.
16	48	0.0237014	-17.	0.0237024	-63.	0.0336232	-30.
$16\frac{2}{3}$	50	0.0237034	-83.	0.0236993	-13.	0.0336224	-23.
$17\frac{1}{3}$	52	0.0237011	-17.	0.0237018	-54.	0.0336226	-29.
18	54	0.0237035	-200.	0.0237003	-21.	0.0336230	-39.
$18\frac{2}{3}$	56	0.0237025	-46.	0.0237012	-38.	0.0336226	-36.
$19\frac{1}{3}$	58	0.0237020	-33.	0.0237018	-88.	0.0336226	-39.
20	60	0.0237020	-38.	0.0237022	-350.	0.0336229	-54.

TABLE II. Emittance data for Case B. $_x = 0.245$; $_y = 0.120$; $= 0.010$

Cumulative values.

Real Ring Time (min)	Million Turns	X_{av}	Doubling Time (days)	Y_{av}	Doubling Time (days)	R_{av}	Doubling Time (days)
$\frac{2}{3}$	2	0.0227520	0.2	0.0192872	0.1	0.0298409	0.1
$1\frac{1}{3}$	4	0.0227605	0.7	0.0193705	0.1	0.0299023	0.1
2	6	0.0227589	1.5	0.0193918	0.1	0.0299149	0.3
$2\frac{2}{3}$	8	0.0227293	−0.3	0.0193824	0.6	0.0298863	−0.8
$3\frac{1}{3}$	10	0.0227243	−0.4	0.0193464	−0.3	0.0298592	−0.4
4	12	0.0227275	−1.3	0.0193089	−0.2	0.0298374	−0.4
$4\frac{2}{3}$	14	0.0227243	2.0	0.0193784	−0.2	0.0298298	−0.5
$5\frac{1}{3}$	16	0.0227431	2.8	0.0192687	−0.2	0.0298235	−0.6
6	18	0.0227731	0.5	0.0192616	−0.3	0.0298419	−2.5
$6\frac{2}{3}$	20	0.0227619	1.1	0.0192598	−0.4	0.0298323	−1.5
$7\frac{1}{3}$	22	0.0227764	0.8	0.0192621	−0.5	0.0298447	37.
8	24	0.0227892	0.6	0.0192630	−0.7	0.0298550	3.1
$8\frac{2}{3}$	26	0.0228057	0.5	0.0192650	−1.0	0.0298687	1.5
$9\frac{1}{3}$	28	0.0228304	0.4	0.0192609	−1.0	0.0298850	1.0
10	30	0.0228423	0.4	0.0192612	−1.3	0.0298944	0.9
$10\frac{2}{3}$	32	0.0228507	0.4	0.0192610	−1.5	0.0299007	1.0
$11\frac{1}{3}$	34	0.0228483	0.5	0.0192603	−1.7	0.0298985	1.3
12	36	0.0228320	1.0	0.0192638	−2.6	0.0298883	2.2
$12\frac{2}{3}$	38	0.0228238	1.5	0.0192628	−2.8	0.0298814	4.2
$13\frac{1}{3}$	40	0.0228216	1.9	0.0192602	−2.6	0.0298782	7.2
14	42	0.0228252	1.9	0.0192582	−2.5	0.0298796	6.9
$14\frac{2}{3}$	44	0.0228277	1.9	0.0192593	−3.2	0.0298822	5.7
$15\frac{1}{3}$	46	0.0228280	2.2	0.0192599	−3.9	0.0298828	6.0
16	48	0.0228312	2.1	0.0192581	−3.6	0.0298841	6.0
$16\frac{2}{3}$	50	0.0228347	1.9	0.0192597	−4.9	0.0298878	4.8
$17\frac{1}{3}$	52	0.0228339	2.4	0.0192654	−26.	0.0298908	4.2
18	54	0.0228401	1.9	0.0192605	−6.7	0.0298924	4.2
$18\frac{2}{3}$	56	0.0228499	1.5	0.0192590	−5.9	0.0298990	3.3
$19\frac{1}{3}$	58	0.0228554	1.5	0.0192570	−5.1	0.0299019	3.1
20	60	0.0228630	1.3	0.0192567	−5.4	0.0299076	2.7

TABLE III. Comparison of double precision and single precision emittance data.

Case A. $\nu_x = \nu_y = 0.245$; $\Delta\nu = 0.010$

Real Ring Time (min)	Million Turns	Single Precision R_{av}	Double Precision R_{av}	Doubling Time Single Precision (days)	Doubling Time Double Precision (days)
2	6	0.0336259	0.0336123	0.01	-6.7
4	12	0.0336252	0.0336288	4.6	1.8
6	18	0.0336260	0.0336277	31.	7.1
8	24	0.0336286	0.0336262	6.7	50.
10	30	0.0336261	0.0336263	-60.	190.
12	36	0.0336251	0.0336253	-21.	-67.
14	42	0.0336246	0.0336241	-23.	-35.
16	48	0.0336220	0.0336232	-10.	-30.
18	54	0.0336232	0.0336230	-24.	-39.
20	60	0.0336237	0.0336229	-52.	-53.
Case B. $\nu_x = 0.245$; $\nu_y = 0.120$; $\Delta\nu = 0.010$					
2	6	0.0298768	0.0298409	-0.9	0.3
4	12	0.0299107	0.0298374	0.7	-0.4
6	18	0.0298781	0.0298419	-0.5	-2.5
8	24	0.0298811	0.0298550	-1.5	3.1
10	30	0.0298718	0.0298944	-1.2	0.9

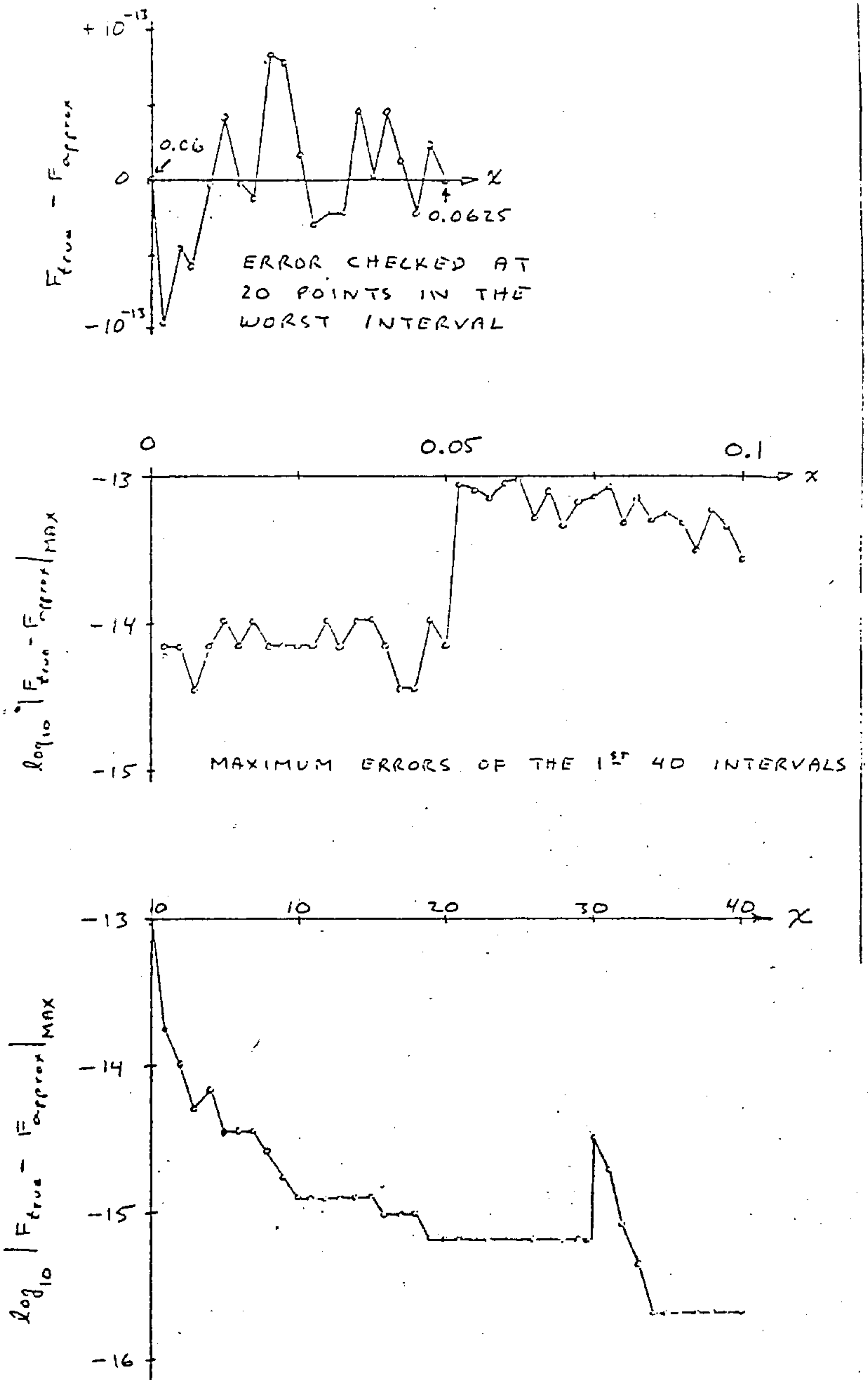

Figure 1. Errors in Single Precision Calculation of F(x,y)

Figure 1A. Double Precision Repeatability Experiment. $\nu_x = \nu_y = 0.245$
Initial Conditions: $X' = Y' = 0$ $\Delta\nu = 0.010$
$X = Y = A\sigma$, where A = 0.5, 1.0, 1.5, 2.0 and where $\sigma = 0.08165$mm.

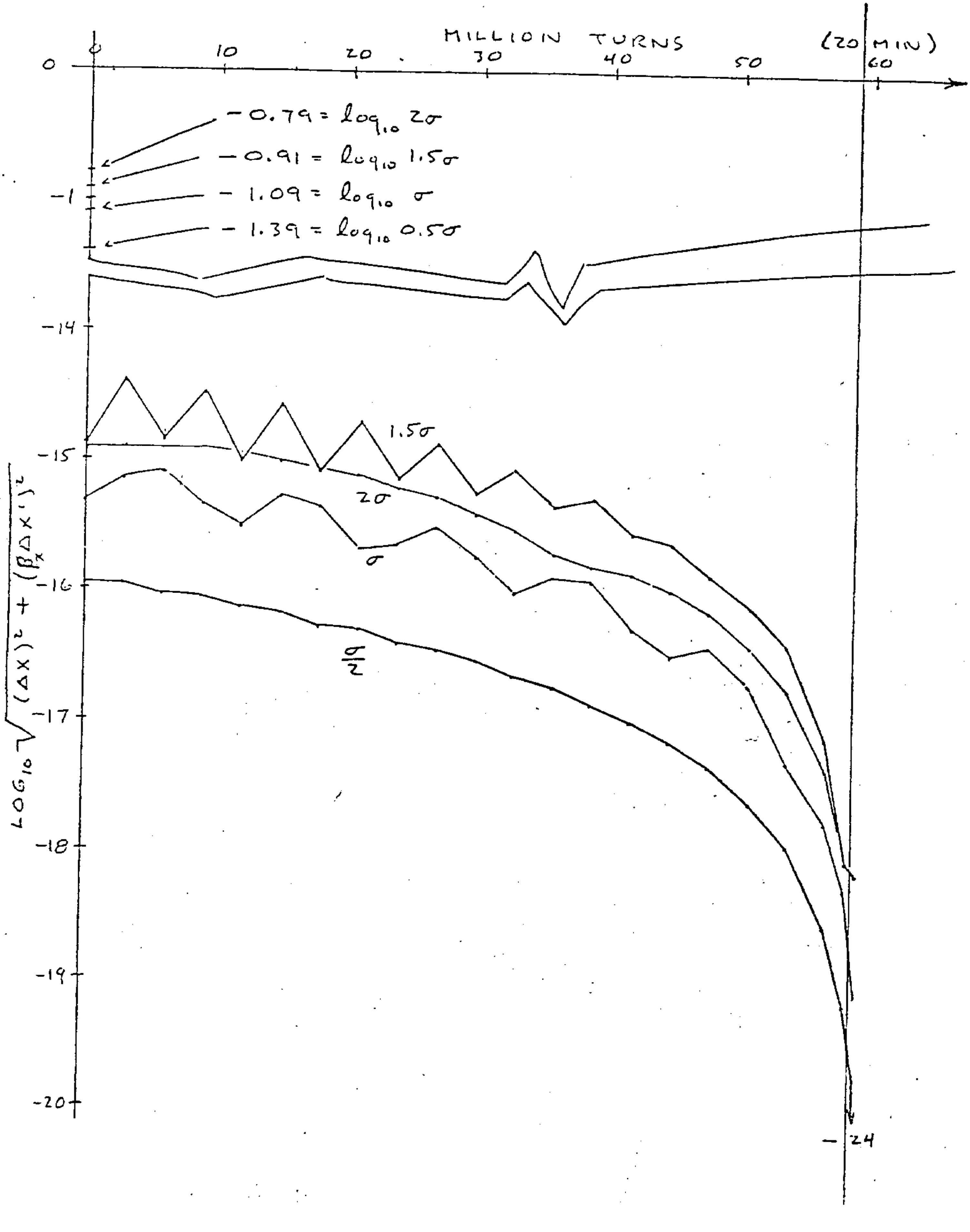

Figure 2. Emittance statistics for Case A

$\nu_x = \nu_y = 0.245; \quad \Delta\nu = 0.010$

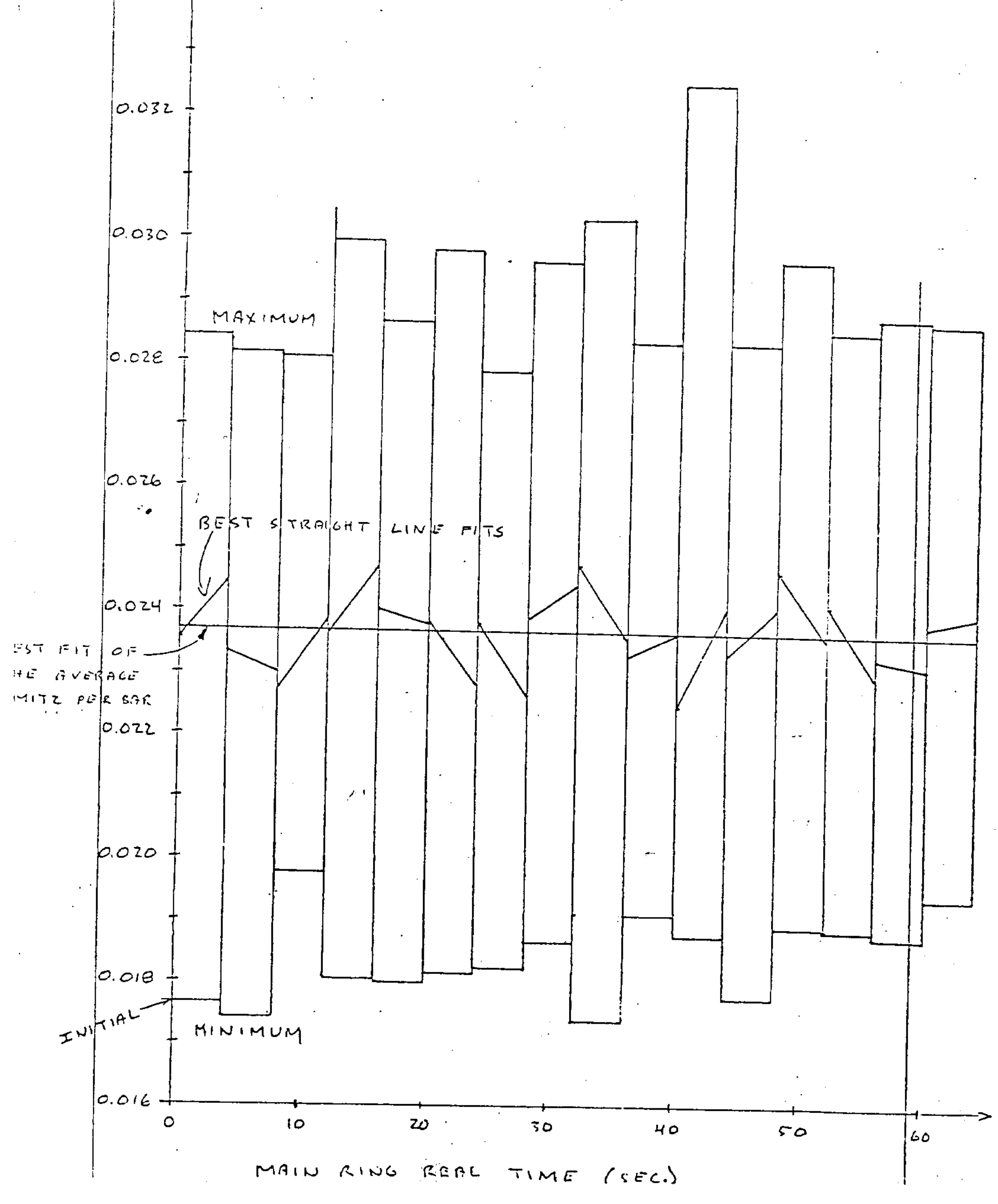

Figure 3. Comparison of x-, y- and R-emittance statistics for Case A; $\nu_x = \nu_y = 0.245$; $\Delta\nu = 0.010$

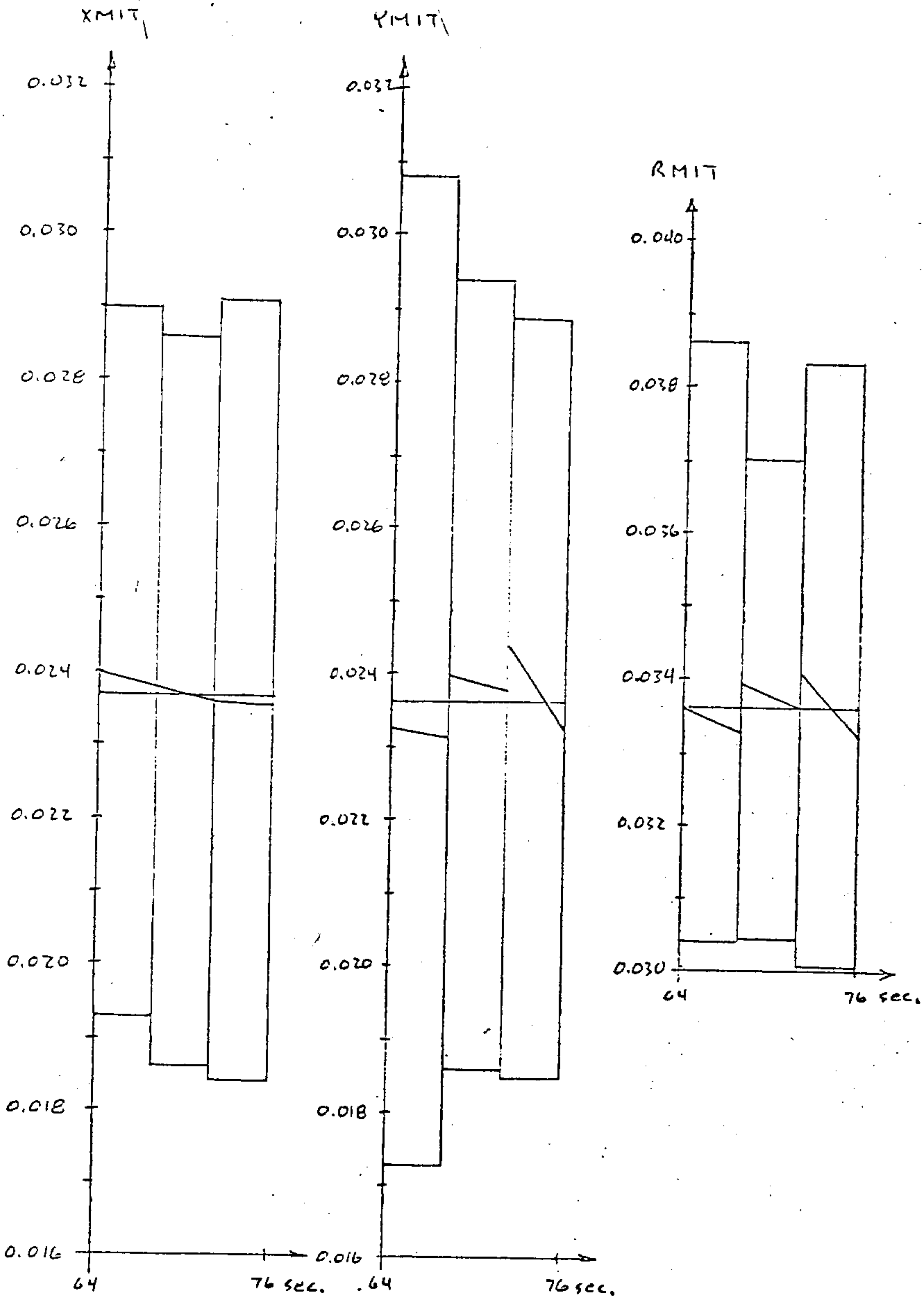

Figure 4. Comparison of x-, y-, and R-emittance statistics for $\nu_x = \nu_y = 0.01617$; $\Delta\nu = 0.010$

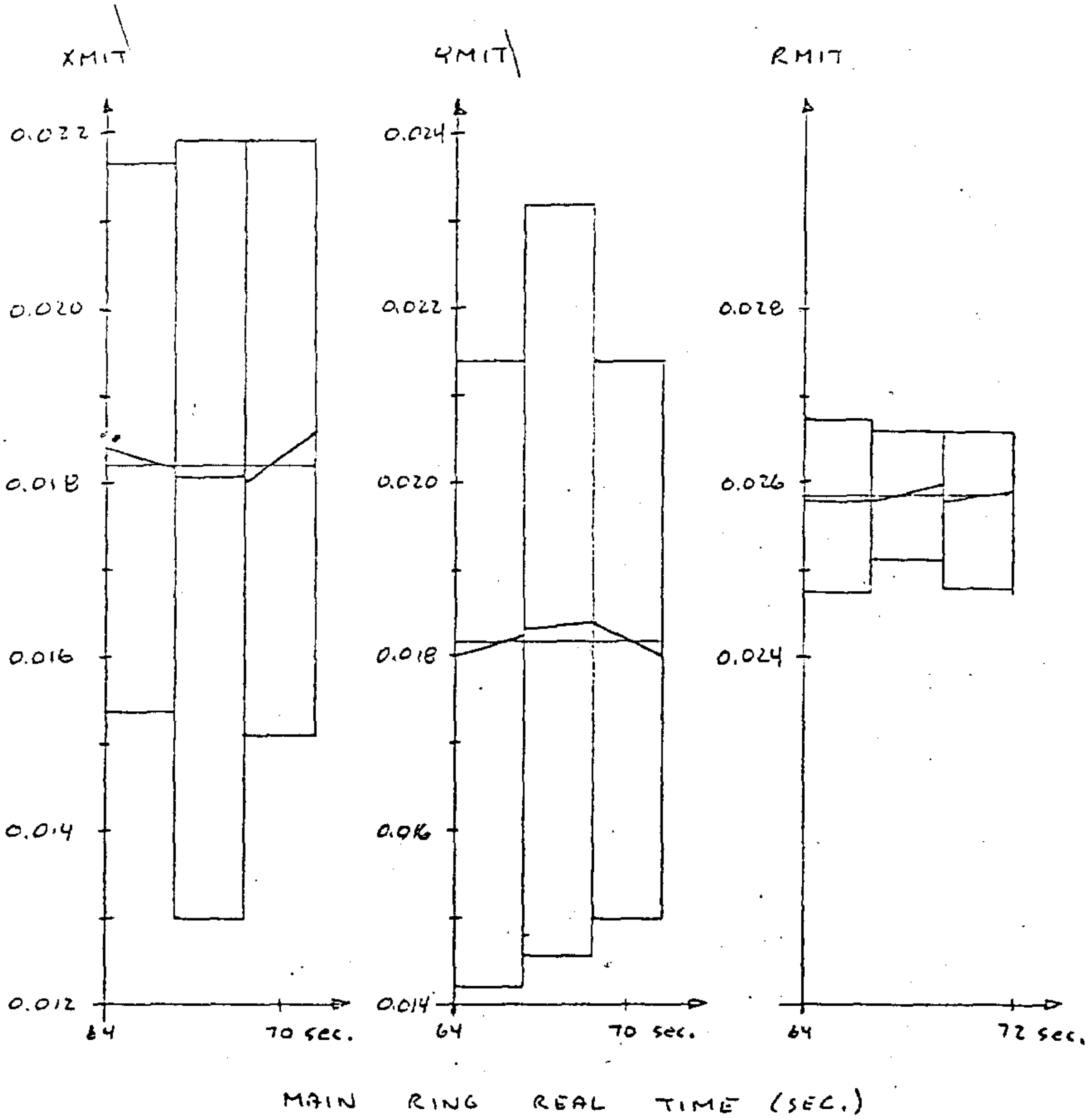

Figure 5. Average values of RMIT from Table I.
Case A. $\nu_x = \nu_y = 0.245$; $\Delta\nu = 0.010$

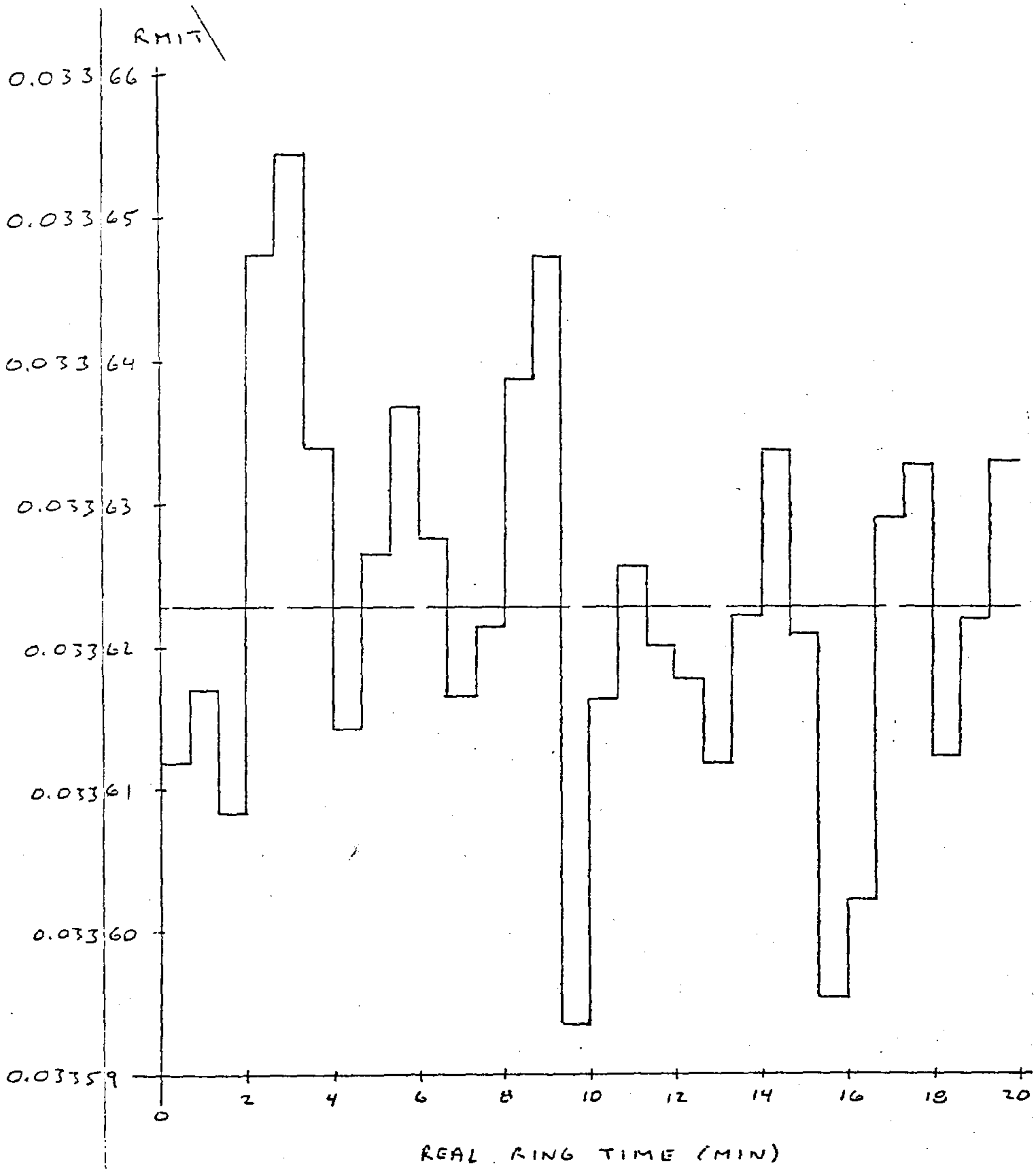

Figure 6. Doubling times for R emittance = $\sqrt{\epsilon_x^2 + \epsilon_y^2}$ from Table I.

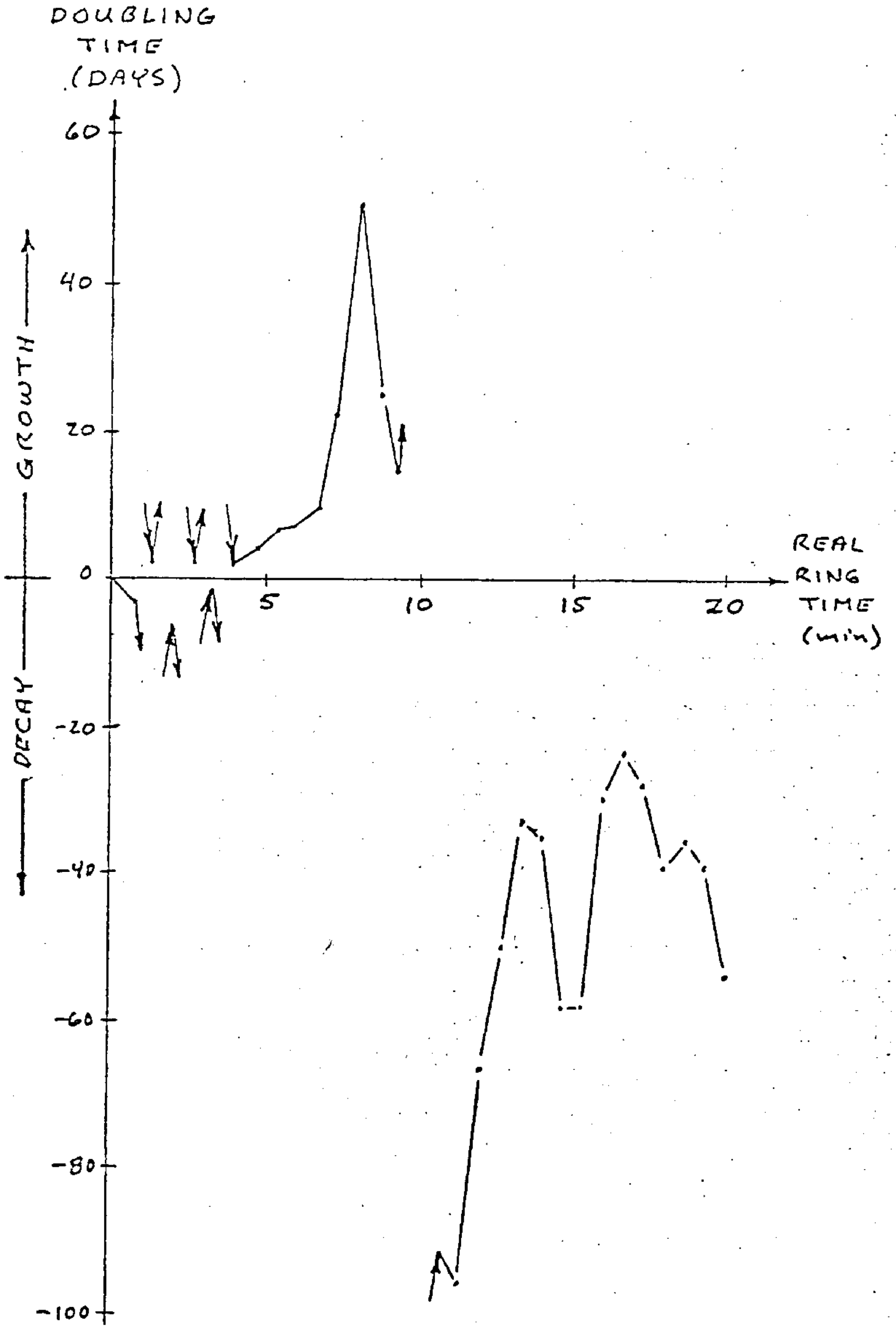

Figure 7. Resonance lines up to 13^{th} order which cross the area in tune space used by Case A. $\nu_x = \nu_y = 0.245$; $\Delta\nu = 0.010$

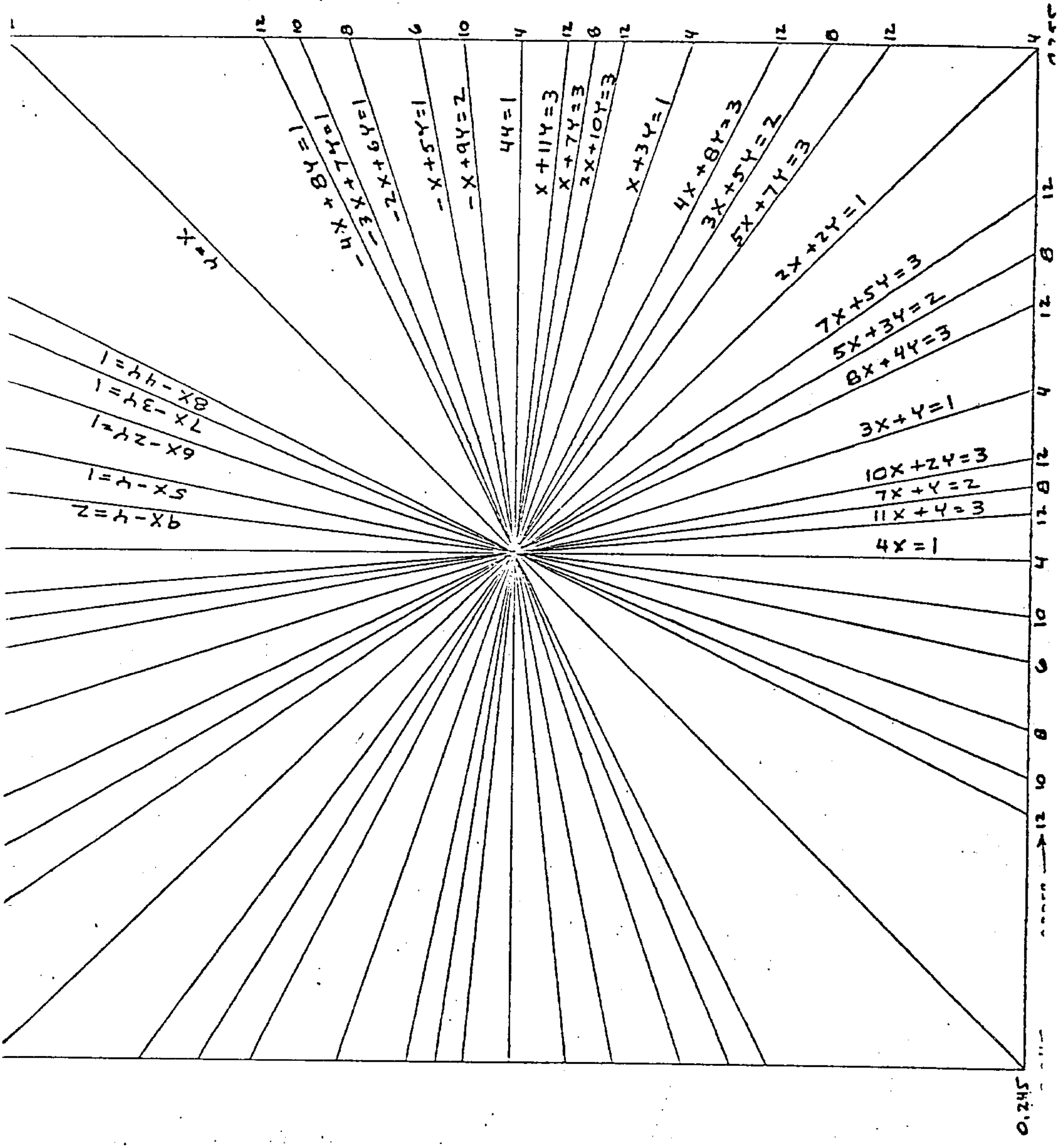

Figure 8. Summary of Table II. Case B. $\nu_x = 0.245$; $\nu_y = 0.120$; $\Delta\nu = 0.010$

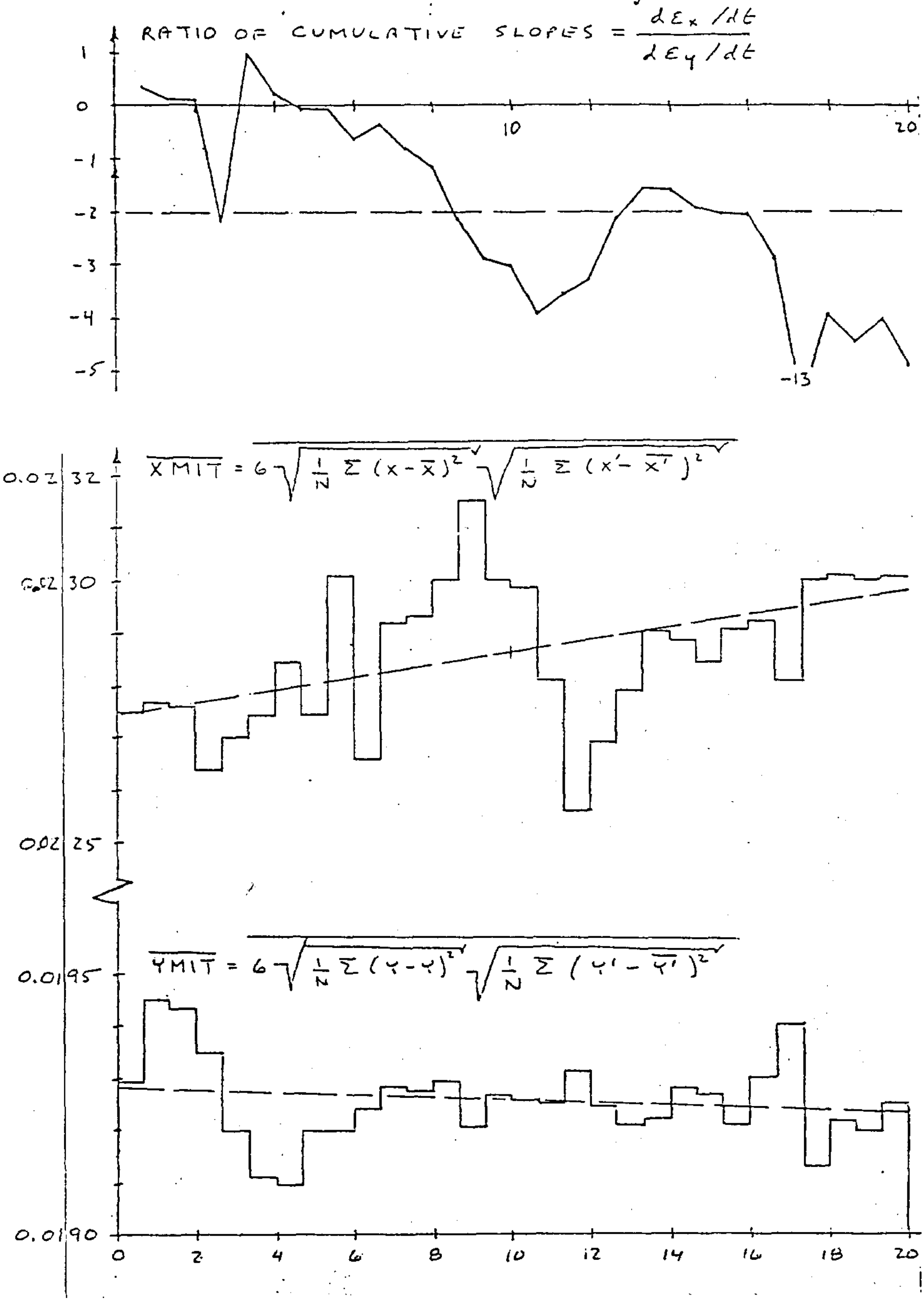

Figure 9. Lines up to 13^{th} order which cross the area in tune space used by Case B. $\nu_x = 0.245$; $\nu_y = 0.120$; $\Delta\nu = 0.010$

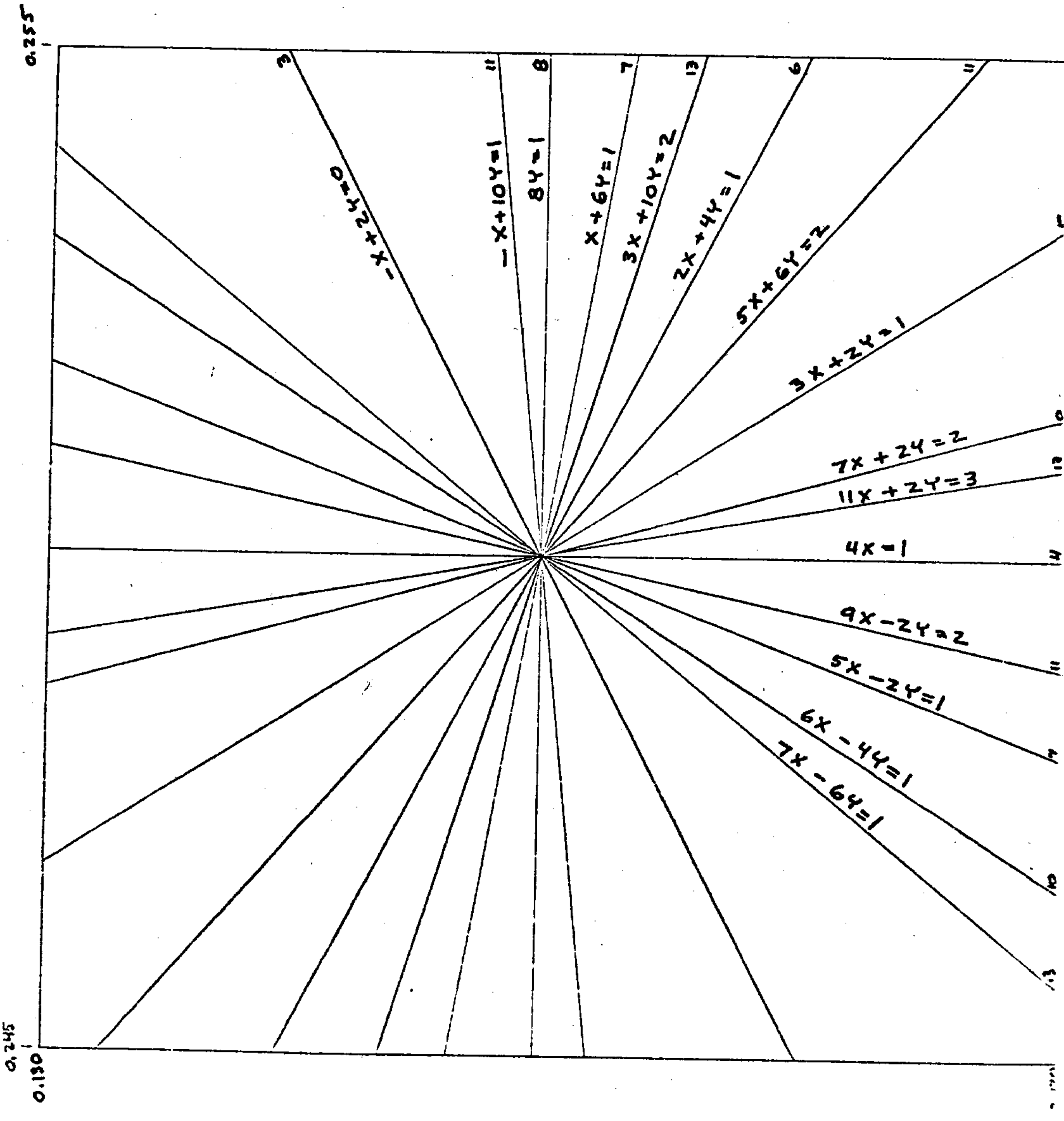

Figure 10. Summary of doubling times in Table II.
Case B. $\nu_x = 0.245$; $\nu_y = 0.120$; $\Delta\nu = 0.010$

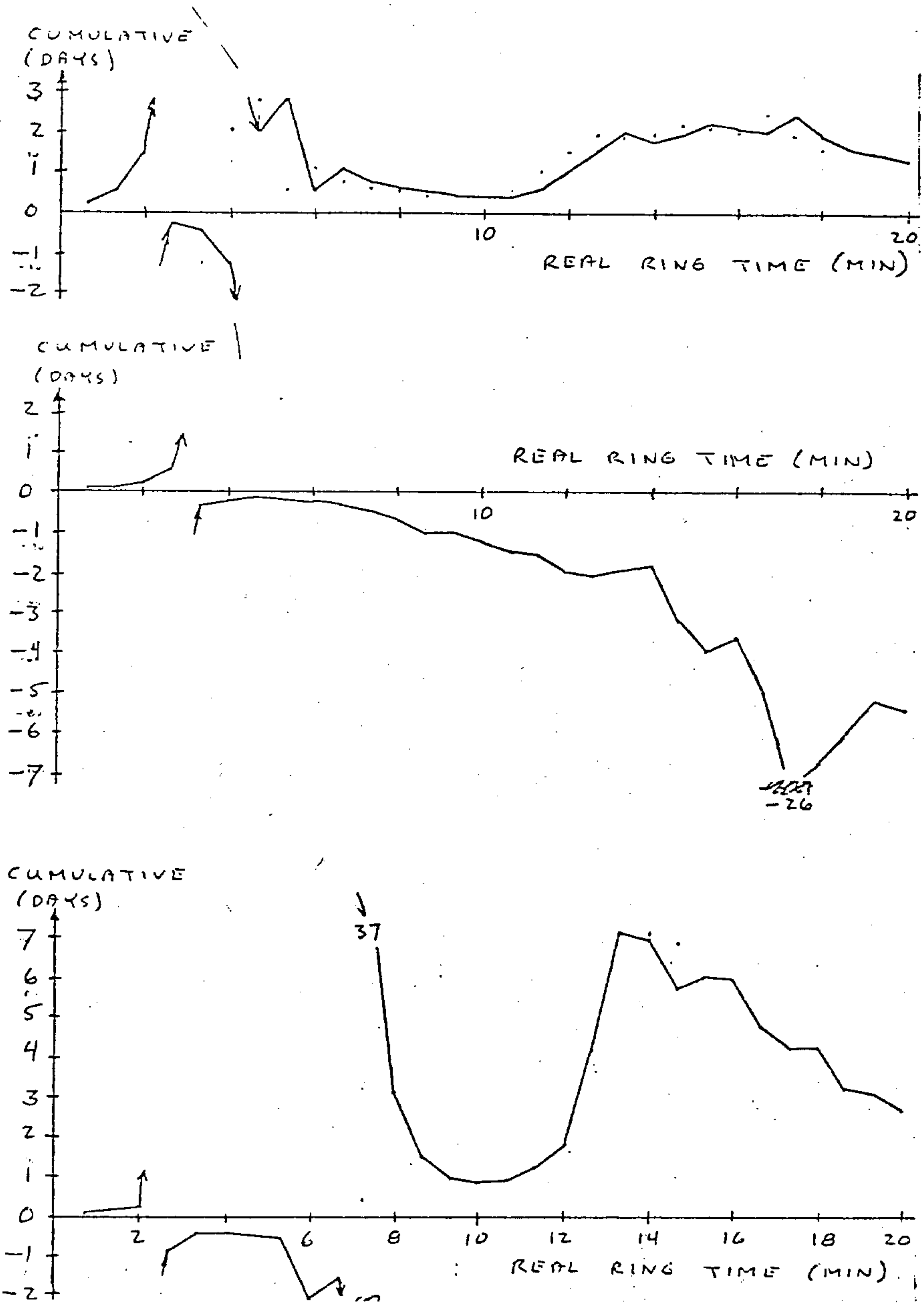

Figure 11. Single Precision Repeatability Experiment. $\nu_x = \nu_y = 0.245$; $\Delta\nu = 0.010$

Initial Conditions: $X' = Y' = 0$

$X = Y = A\sigma$, where $A = 0.5, 1.0, 1.5, 2.0$; $\sigma = 0.08165$

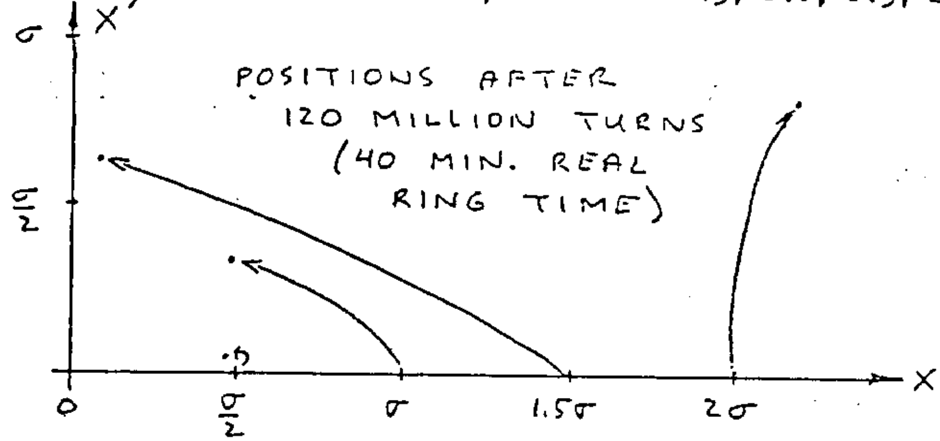

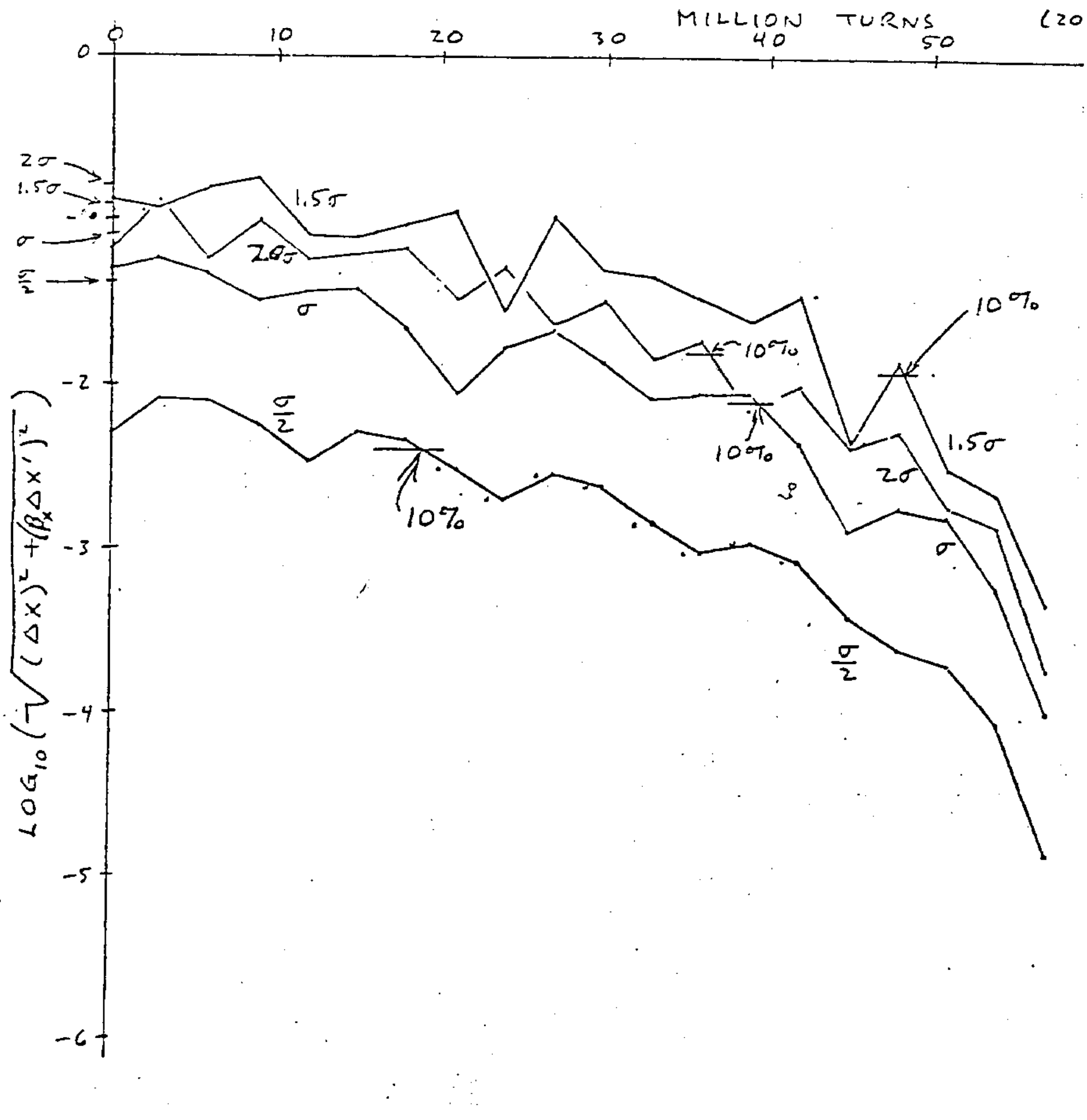

Figure 12. Definition of terms used in the emittance statistics.